Synthesis of CQD-Decorated ZnO Nanoflowers for Efficient Photocatalytic Remediation of Organic Pollutants

A Dissertation

Submitted for the partial fulfillment

of

the award of the degree of

MASTERS OF SCIENCE

In

CHEMISTRY

By

Hitesh Bansal

(Reg. No: 302302003)

Under the supervision of

Dr. SOUMEN BASU

Professor

THAPAR INSTITUTE
OF ENGINEERING & TECHNOLOGY
(Deemed to be University)

Department of Chemistry and Biochemistry

Thapar Institute of Engineering and Technology

Patiala-147004, Punjab

June 2025

Certificate

This is to certify that the dissertation entitled ***"Synthesis of CQD-Decorated ZnO Nanoflowers for Efficient Photocatalytic Remediation of Organic Pollutants"*****,** submitted by **Hitesh Bansal to the Department of Chemistry and Biochemistry, Thapar Institute of Engineering and Technology, Patiala,** in partial fulfillment of the requirements for the award of the degree of **Master of Science in Chemistry**, is a genuine and original record of the research work carried out under my supervision.

To the best of my knowledge, the candidate has adhered to all guidelines and procedures for the submission of this dissertation, and the work presented meets the academic standards prescribed by the institute. Furthermore, this dissertation has not been submitted, either partially or wholly, to any other university or institute for the award of any other degree or diploma.

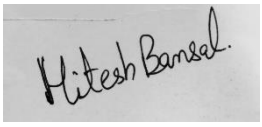

Date: 23-06-2025 **HITESH BANSAL**

Place: TIET, Patiala. **(302302003)**

It is certified that the aforementioned statement made by the student is correct to the best of my knowledge and belief.

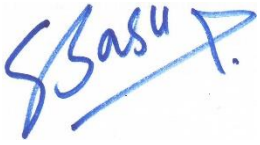

Dr. Soumen Basu

Professor

Department of Chemistry and Biochemistry

Thapar Institute of Engineering and Technology, Patiala

CANDIDATE'S DECLARATION

I hereby declare that the dissertation entitled ***" Synthesis of CQD-Decorated ZnO Nanoflowers for Efficient Photocatalytic Remediation of Organic Pollutants"*,** submitted in partial fulfillment of the requirements for the award of the degree of **Master of Science in Chemistry to the Department of Chemistry and Biochemistry, Thapar Institute of Engineering and Technology, Patiala,** is a bona fide record of my own work carried out under the supervision of **Dr. Soumen Basu,** Professor, Department of Chemistry and Biochemistry, Thapar Institute of Engineering and Technology. I further declare that this work has not been submitted, either in part or in full, to any other university or institution for the award of any other degree or diploma.

Date: 23-06-2025 **HITESH BANSAL**

Place: TIET, Patiala. **(302302003)**

ACKNOWLEDGEMENT

First and foremost, I would like to express my heartfelt gratitude to **God** for granting me the strength, patience, and determination to successfully complete this project.

I extend my deepest and sincerest gratitude to my project supervisor, **Dr. Soumen Basu,** Professor, Department of Chemistry and Biochemistry, Thapar Institute of Engineering and Technology, Patiala. His unwavering support, continuous motivation, and insightful guidance have been instrumental in the successful completion of this project. I am truly grateful for the opportunity to work under his mentorship, which consistently directed and encouraged me throughout the research journey.

I am immensely grateful to **Dr. Manmohan Chhibber,** Professor and Head of the Department of Chemistry and Biochemistry, for granting me the opportunity to undertake this dissertation project. I also extend my heartfelt appreciation to all the faculty members and staff of the Department of Chemistry and Biochemistry (DCBC) for their continuous support, encouragement, and guidance throughout this journey.

I am deeply grateful to **Ms. Palkaran Sethi** for their unwavering support, profound understanding, and extensive expertise. Their sincerity, patience, and warm-hearted nature have been a constant source of inspiration. Their thoughtful suggestions, offered with kindness and encouragement, have played a pivotal role in the smooth and successful completion of this project.

I am filled with profound gratitude towards my lab seniors for their cooperative guidance, approachable nature, and invaluable assistance throughout the course of my project.

I also extend my sincere thanks to **Thapar Institute of Engineering and Technology and the Department of Chemistry and Biochemistry** for their generous funding and for providing the essential infrastructure and research facilities that enabled me to carry out my experiments successfully.

Lastly, and most importantly, I am deeply thankful to **my parents, family, and friends** for their unconditional love, unwavering support, heartfelt prayers, and constant encouragement in every aspect of my life.

Table of Contents

List of figures

List of Tables.

List of schemes.

List of Abbreviations

Z	ZnO
Q	CQD's
ZQ	ZnO-CQD's nanocomposite

MB	Methylene Blue
XRD	X-Ray Diffraction
XPS	X-Ray Photoelectron Spectroscopy
FE-SEM	Field Emission Scanning Electron Microscopy
EDS	Energy-dispersive X-Ray Spectroscopy
PL	Photoluminescence Spectroscopy
BET	Brunauer–Emmett–Teller
UV-Vis	Ultraviolet- Visible
DRS	Diffuse Reflectance Spectroscopy
TOC	Total Organic Carbon
COD	Chemical Oxygen Demand
FTIR	Fourier Transmission Infrared Spectroscopy
LC-MS	Liquid Chromatography Mass Spectrometry
HR-TEM	High Resolution Transmission Electron Microscopy
Ev	Electron Volt
Λmax	Absorption Maxima
wt.	Weight
m^2/g	Meter Square Per Gram
Nm	Nanometer
^{0}	Degree Celsius
Ml	Milliliter
a.u.	Arbitrary units
g/l	Gram per liter
H	Hours
Min	Minutes
Mg	Milligram
PCS	Porous Carbon Spheres

Abstract

A heterostructured ZnO–Carbon Quantum Dot (CQD's) nanocomposite was successfully synthesized with varying CQD's loadings (5%, 10%, and 15%) to develop an efficient and reusable photocatalyst for environmental remediation. The composite exhibited a distinctive nanoflower-like ZnO morphology uniformly decorated with CQD's, forming a robust heterojunction that enhanced visible light absorption, promoted efficient charge separation, and facilitated easy catalyst recovery. Comprehensive material characterization using XRD, FTIR, XPS, BET, PL, UV-DRS, FESEM, EDS, and HR-TEM confirmed its high crystallinity, surface area, and sunlight responsiveness. Photocatalytic performance evaluated under natural sunlight demonstrated an impressive 97.7% degradation of methylene blue within 60 minutes, following pseudo-first-order kinetics with a rate constant of 0.047 min^{-1}—over five times higher than commercial TiO_2-P25. The influence of operational parameters such as pH, light source, catalyst dosage, and reactive species was systematically assessed. The catalyst maintained high stability and reusability, retaining 85% efficiency after six cycles. LC-MS analysis revealed intermediate degradation products, while TOC and COD assessments confirmed substantial mineralization. Given the environmental persistence and toxicity of methylene blue, the ZnO-CQD composite presents a sustainable, solar-driven approach for treating dye-contaminated wastewater with high efficiency and recyclability.

Keywords: ZnO-Carbon Quantum Dots, Binary nanocomposite, organic pollutant degradation, Photocatalytic degradation, Pseudo-first order kinetics.

CHAPTER 1 – INTRODUCTION

1.1 Basic Frame

As cities grow and more people move into urban areas, the need for clean water is rising faster than ever, leading to serious shortages and making it clear that tackling water scarcity is more urgent than ever before[1]. The water scarcity crisis is further compounded by the pollution of natural water bodies, particularly through the discharge of industrial contaminants such as synthetic dyes, heavy metals, and various organic substances, which significantly reduce the accessibility of clean and safe drinking water [2]. Synthetic dyes are extensively applied across multiple industries due to their durability and resistance to environmental and chemical stress [3].

1.2 Methylene Blue (MB) – A Blue Colored Pollutant

Methylene blue is widely used in various industries, but its high concentration in the environment presents significant health and ecological risks. In humans, exposure can cause skin and eye irritation, respiratory problems, and, in severe cases, hemolytic anemia, especially in individuals with glucose-6-phosphate dehydrogenase deficiency. Environmentally, MB is persistent and resists natural degradation, negatively affecting aquatic organisms by disrupting photosynthesis and oxygen exchange. Its potential carcinogenicity further emphasizes the need for effective removal methods from wastewater to protect both human health and ecosystems [4–6]. The structure for the Methylene Blue is shown in Figure 1.

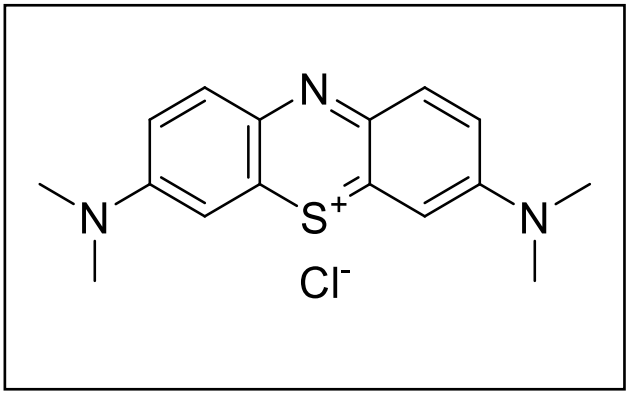

Figure 1. Structure of Methylene Blue Dye.

1.3 Practices for waste water treatment

Various wastewater treatment methods, including biological adsorption, chemical oxidation, and physical filtration, have been widely used for dye removal. Biological processes like activated sludge systems can handle some basic dyes but are often ineffective against complex dye structures and involve slow removal kinetics [7]. Chemical oxidation methods, while capable of degrading dye molecules, typically require high operational costs and strict control conditions [8]. Physical treatments such as ultrafiltration offer significant dye rejection but face challenges like membrane fouling and substantial energy consumption [9] and adsorption [10]. Due to these limitations—including incomplete degradation, secondary pollution, and energy-intensive operation—there is a growing demand for more sustainable, efficient, and environmentally friendly approaches to address wastewater contamination [11].

1.4 Photocatalytic degradation and some heterojunction photocatalysis

Photocatalytic degradation stands out as a highly sustainable and eco-friendly approach for eliminating pollutants, harnessing the energy of UV-visible light without generating harmful byproducts. This method effectively breaks down organic contaminants into harmless end products like CO_2 and H_2O [12] making it an attractive solution for treating a broad spectrum of pollutants. However, the success of this process relies heavily on the development of an efficient photocatalyst—one that can be activated under UV-visible light. To achieve optimal performance, it is essential to design photocatalysts with a low energy band gap, a large surface area, and minimal charge carrier recombination, ensuring faster and more complete degradation of pollutants.

Zinc oxide (ZnO) has gained significant attention due to its outstanding optical, structural, and electrical properties, making it a prime candidate for various nanotechnology applications [13]. Nanocrystalline ZnO thin films prepared at different substrate temperatures showed that higher temperatures promote crystallinity and widen the band gap, typically ranging from 3.2 to 3.4 eV [14]. ZnO nanorods grown on p-type silicon demonstrated electrical bi-stability and negative differential resistance, largely due to oxygen vacancies and interstitial defects [15]. Similarly, tetrapod-shaped ZnO nanostructures exhibited strong UV emission at 380 nm and defect-related emissions, with their electrical properties varying according to growth density and temperature [16]. Advanced hydrothermal techniques enabled the fabrication of dense ZnO nanorods and

nanoflowers, where strong near-band-edge emissions confirmed high optical quality with minimal deep-level defects [17]. Despite their promising properties, ZnO nanoparticles pose environmental risks, exhibiting antibacterial activity through the generation of reactive oxygen species (ROS) under light, and even some toxicity in dark conditions [18]. Thus, while ZnO nanomaterials show tremendous potential for optoelectronic and photocatalytic applications, careful attention must be given to their environmental impact.

Due to their special optical and electrical properties, a new class of Carbon quantum dots (CQD's) have shown great potential in different applications including photocatalysis, bioimaging and sensing. They are promising candidates in next-generation photocatalytic devices due to their high efficiency to harvest solar light and promote the separation of charges. add a word a novel type of carbon quantum dots [19]. Strong optical absorption, adjustable photoluminescence, superior redox activity, and effective charge transfer are characteristics of carbon-based quantum dots, including carbon and graphene variations. These characteristics make them very efficient photocatalysts, especially for uses like water splitting and CO_2 reduction triggered by visible light [20]. Ultrasmall carbon compounds with highly adjustable optical characteristics, carbon quantum dots (CQD's) hold promise for uses such as photocatalysis. Strategies like size control, surface functionalization, elemental doping, and forming 0D/2D heterojunctions with materials like graphene, metal oxides, and graphitic carbon nitride can greatly increase their photocatalytic efficiency, allowing for efficient solutions for CO_2 reduction, hydrogen generation, and pollutant degradation [21]. An example of CQD's application is the synthesis of ultrasmall BiOI nanosheets assembled into hollow microspheres using a [Bmim]I-assisted method at room temperature. The introduction of CQD's enhanced full-spectrum light absorption, enlarged surface area, and improved electron–hole separation, leading to superior photocatalytic degradation of TC, BPA, and RhB. This strategy showcases how CQD's can effectively tailor nanostructures and boost photocatalytic activity [22]. Another noteworthy instance is the creation of a CQD's/$ZnFeO_4$ composite using a straightforward hydrothermal process, which demonstrated an eight-fold greater photocurrent responsiveness than that of pure $ZnFeO_4$. The use of CQD's improved electron–hole separation and served as an electron reservoir, which greatly increased the elimination of NO_x under visible light. This illustrates how CQD's can enhance air purification applications and increase photocatalytic efficiency [23].

1.5 Present Work

Using a hydrothermal process, ZnOCQD's nanocomposites in different ratios were created for this study. The produced photocatalysts were tested for their ability to effectively combat the organic pollutant methylene blue (MB) by photocatalytic degradation assays carried out in the presence of natural sunshine. Numerous investigations were conducted, including kinetic analyses, catalyst dosage optimization, scavenger analysis, the impact of pH, and reusability testing. Relative efficiency was evaluated by comparing the photocatalytic performance with the commonly used TiO_2-P25. Additional mineralization tests were conducted, and the degradation products were analyzed using liquid chromatography–mass spectrometry (LC–MS). A believable photocatalytic degradation process was suggested in light of the findings.

1.6 Thesis objective

Our basic strategy was on creating a nanocomposite that can efficiently eliminate hazardous organic contaminants from wastewater. This was accomplished by incorporating CQD's onto ZnO, which led to the creation of a very effective wastewater treatment heterojunction nanocomposite. Using sophisticated methods like FTIR, UV-DRS, X-ray diffraction (XRD), and Brunauer–Emmett–Teller (BET) analysis, the structure and composition of the nanocomposite were carefully described. In order to comprehend the nanocomposite's potential for photocatalytic activity under visible and UV light irradiation, UV-DRS (Ultraviolet Diffuse Reflectance Spectroscopy) is essential since it offers useful information on the material's light absorption characteristics. X-ray Photoelectron Spectroscopy (XPS) was used to analyze the elemental oxidation states, and Field Emission Scanning Electron Microscopy (FESEM) was used to analyze the morphology. Utilizing High-Resolution Transmission Electron Microscopy (HR-TEM), the precise structure was evaluated at the nanoscale as well. Additionally, the electrical characteristics of the nanocomposite were assessed using Photoluminescence (PL) spectroscopy. To provide an accurate understanding of the photocatalysts' performance, a variety of investigations were carried out to compare their ability to absorb and decomposition capacities under varied circumstances.

CHAPTER 2 – LITREATURE REVIEW

The successful creation of nanocomposites based on ZnO and carbon quantum dots (CQD's), which display a range of structural shapes, surface properties, and particle sizes, has been shown in numerous investigations. These hybrid materials have demonstrated promising performance in a variety of applications, most notably the sensitive detection of harmful heavy metal ions in environmental situations and the destruction of toxic organic pollutants.

Enhancing dye degradation has been achieved through the integration of ZnO with carbon quantum dots generated from ascorbic acid. Wider light absorption and increased photocatalytic efficiency under illumination are the results of the substantial facilitation of photoinduced charge carrier separation provided by the presence of CQD's on the ZnO surface.

A recent study used a straightforward co-precipitation method to investigate the production of La-doped ZnO photocatalysts. The successful La^{3+} doping and the retention of the ZnO wurtzite phase were confirmed by structural investigation using XRD. Under solar light, the 5% La-doped ZnO demonstrated a much higher photocatalytic performance, degrading methylene blue (MB) by 98% in 90 minutes as opposed to 51% for pristine ZnO. Reduced charge carrier recombination, as shown by quenched PL spectra, was the main cause of this improvement. Additional validation of the elemental composition and doping effects was obtained using XPS analysis. Effective charge transport behavior was demonstrated by the doped nanostructures. Studies on reusability revealed that the photocatalyst remained active for four cycles. These results demonstrate how La doping can improve ZnO-based photocatalysts [24].

In another study it has been shown that to improve ZnO-based photocatalysts for wastewater purification by adding non-metal dopants. One such attempt used 1% and 5% sulfur concentrations to create S-doped ZnO thin films via a seed-mediated hydrothermal process. Sulfur boosted ZnO's crystallinity and changed its shape, which enhanced its photocatalytic capabilities. With a reaction rate of 1.67×10^{-2} min^{-1}, these S-doped films were able to degrade Rhodamine B (RhB) by up to 92% when exposed to visible light. Less charge carrier recombination is thought to be the cause of the increased activity. Additionally, the catalyst showed good stability, maintaining 75%

efficiency across several cycles. These results highlight sulfur-doped ZnO's potential as an efficient and reusable photocatalyst for environmental uses [25].

Recently, graphene oxide (GO)-based nanocomposites containing ZnO and metal nanoparticles have shown promise as photocatalysts. A recent work used a simple one-pot approach to create GO/ZnO nanocomposites embedded with metal nanoparticles. XRD, SEM, and FTIR characterization verified the composites' structure and production. By breaking down methylene blue (MB) in the presence of sunshine, the photocatalytic activity was evaluated. With 3.125% GO, 84% degradation was achieved in 90 minutes. Copper and silver were added as metal dopants to investigate further improvement. In only 40 minutes, GO-ZnO-Ag accomplished total MB degradation, whereas GO-ZnO-Cu demonstrated decreased efficiency. These results demonstrate how well silver-doped GO–ZnO composites work in wastewater treatment applications. Nevertheless, even with its superior efficiency, the inclusion of silver raises the total cost considerably, which restricts its scalability for treating wastewater on a big scale [26].

In Malaysia, empty fruit bunches (EFB), a significant agricultural waste, offer a useful carbon-rich feedstock for the synthesis of nanomaterials. Hydrothermal treatment of EFB-derived lignin was used to create nitrogen-doped carbon quantum dots (NCQD’s) in a sustainable manner. Strong blue fluorescence was displayed by these NCQD’s, which remained optically stable even after eight months of storage and extended UV exposure. With an average size of 3.6 nm, the synthesized particles showed remarkable photocatalytic activity by breaking down 97% of methylene blue and 98% of malachite green in 180 and 120 minutes, respectively, when exposed to sunshine. According to the Langmuir-Hinshelwood model, the deterioration proceeded according to first-order kinetics. This study provides a promising answer for dye removal in water treatment applications by demonstrating an eco-friendly and effective method of creating NCQD’s [27].

Although ZnO is frequently employed as an industrial photocatalyst, it has trouble degrading antibiotics that are difficult to break down in wastewater. A unique ZnO/N,S-CQD’s hybrid nanoflower was created by embedding surface-functionalized nitrogen and sulfur co-doped carbon quantum dots (N,S-CQD’s) into ZnO using a straightforward one-pot hydrothermal technique. Under visible and near-infrared light, the resultant photocatalyst demonstrated noticeably better performance, achieving 72.8% MG degradation in 180 minutes. The highly reactive facets of ZnO

in conjunction with the up-converted luminescence and effective electron transfer characteristics of N,S-CQD's are responsible for this amplification. Experiments using active species trapping showed that the degradation pathway involved superoxide anions, holes, and hydroxyl radicals. Furthermore, when applied to actual water samples, the photocatalyst maintained an efficacy of over 60%, indicating its great promise as an inexpensive and highly efficient material for industrial antibiotic breakdown under sunlight [28].

Using a hydrothermal process, a new TiO_2-based composite containing nitrogen-doped carbon quantum dots (NCQD's) was created and used for photocatalytic NO degradation in both visible and ultraviolet light. With a 27% conversion rate under visible light, the P25/NCQD's composite showed a significant improvement in NO removal efficiency, more than double that of bare P25. Furthermore, the reaction's selectivity considerably increased. The combination also functioned better than pure P25 under UV radiation, showing notable improvements in selectivity and conversion rate. Additionally, methylene blue's photocatalytic degradation was greatly enhanced, increasing from 68% (P25) to 91% in just one hour of UV exposure. This increased activity is ascribed to the function of NCQD's, which accelerate charge separation and transfer, decrease electron-hole recombination, and prolong visible light absorption [29].

When compared to the research included in Table 1, it is evident that the catalyst created in our investigation performs better than systems that have been previously published, achieving high efficiency even at relatively lower dosages. It has been shown that adding CQD's to the ZnO matrix is an extremely effective approach that greatly increases photocatalytic activity. Among the numerous catalysts that have been published, this synergistic combination stands out, highlighting its potential to provide superior degrading performance in wastewater treatment applications.

Table1. List of various ZnO, CQD's based nanocomposites reported in the literature.

Photocatalyst	Pollutant	Reaction Time (min^{-1})	References
La doped ZnO	Methylene Blue	90	[24]
S doped ZnO	Rhodamine B	150	[25]
GO/ZnO	Methylene Blue	90	[26]
N doped CQD's	Methylene Blue Malachite Green	180 120	[27]
ZnO/N,S-CQD's	Malachite Green	180	[28]
TiO2/NCQD's	Methylene Blue	60	[29]

CHAPTER 3 – Zinc Oxide-Carbon Quantum Dots Nanocomposites

3.1 Materials and Methodology

3.1.1. Chemical and Materials

Zinc nitrate hexahydrate (Zn $(NO_3)_2 \cdot 6H_2O$), L-Ascorbic acid, Sodium Hydroxide (NaOH), and Methylene Blue powder were obtained from Loba Chemie. The solutions were prepared by using the ultrapure double distilled water. Pure reagents were used without any adulteration.

3.1.2. Synthesis of Zinc Oxide (ZnO)

To create ZnO nanoparticles (abbreviated Z), 4.46 grams of zinc nitrate hexahydrate were first dissolved in 30 milliliters of distilled water while being constantly stirred for 30 minutes to guarantee the salt was completely dissolved. With continuous stirring, the pH of the resultant solution was gradually brought down to 12 by adding 5 M sodium hydroxide solution dropwise. The homogenous mixture was then moved to a stainless-steel autoclave lined with Teflon and hydrothermally treated using a muffle furnace for two hours at 125°C, in accordance with previously documented procedures [30]. After the reaction was finished, centrifugation was used for three minutes at 6000 rpm to separate the ZnO precipitate. To get rid of unreacted precursors and contaminants, the recovered product was carefully cleaned many times using distilled water and ethanol. In order to prepare them for additional characterization, the purified ZnO nanoparticles were lastly allowed to air dry at ambient temperature.

3.1.3. Synthesis of Carbon Quantum Dots (CQD's)

Carbon quantum dots (abbreviated as Q), were created by fully dissolving 2 grams of L-ascorbic acid in 20 milliliters of distilled water at room temperature. After that, the resultant solution was put into a stainless-steel autoclave lined with Teflon and heated to 180°C for eight hours in a muffle furnace. The process ended with the formation of a light-yellow suspension. Any residues or unreacted material were removed from this suspension by filtering it using regular filter paper. The carbon quantum dots were present in the light brown filtrate, whereas the solid residue that remained on the filter paper was disposed of [31].

3.1.4. Synthesis of ZnO-CQD's nanocomposite

In a beaker, 950 mg of synthesized ZnO and 10 mL of CQD's solution were mixed to create the ZnO-CQD's nanocomposites. To guarantee complete interaction between the two ingredients, the mixture was agitated overnight at room temperature. This made it easier for CQD's to be evenly distributed across the ZnO surface. The solid product was collected by centrifuging the suspension after it had been sufficiently mixed. To get rid of any remaining contaminants, the precipitate was then repeatedly cleaned using ethanol and distilled water. To create a stable powder, the purified composite was dried in a hot air oven for the entire night. The final product's CQD's content led to its designation as ZQ5. ZQ10 and ZQ15 were among the other nanocomposites that were created by altering the volume of CQD's solution. A comparison of the effects of CQD's loading on photocatalytic performance was made possible by these differences. Scheme 1 shows a schematic representation of the synthesis pathway.

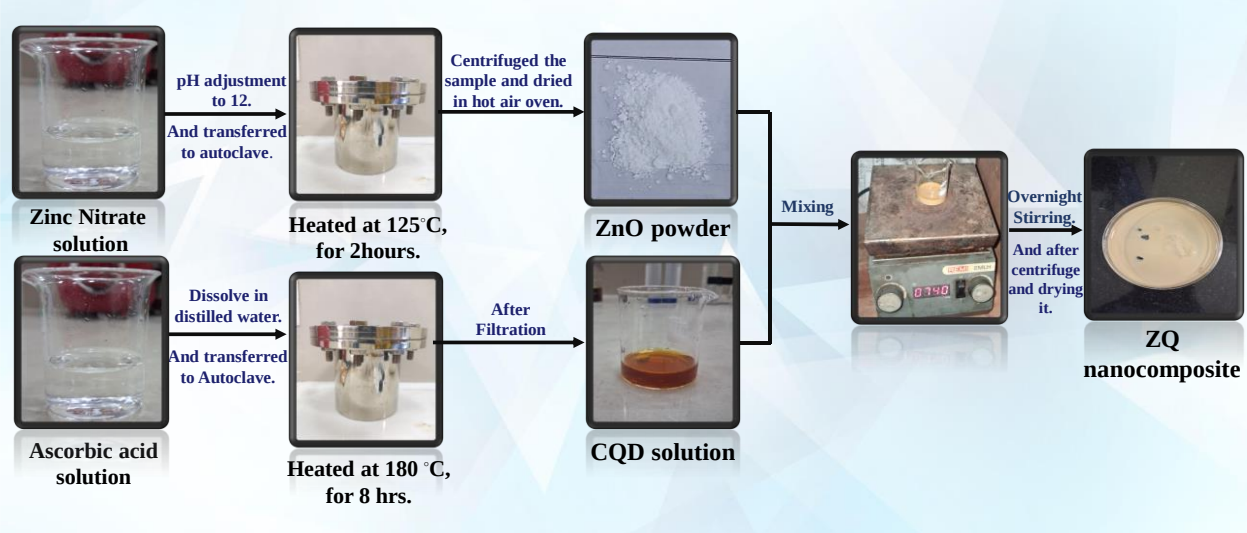

Scheme 1. Synthesis of ZnO-CQD's nanocomposite

3.2 Results and Discussions

3.2.1 XRD analysis

X-ray diffraction is widely used to examine the purity of crystal structure. XRD analysis was done for the bare materials Z, Q and for the nanocomposites ZQ5, ZQ10 and ZQ15.

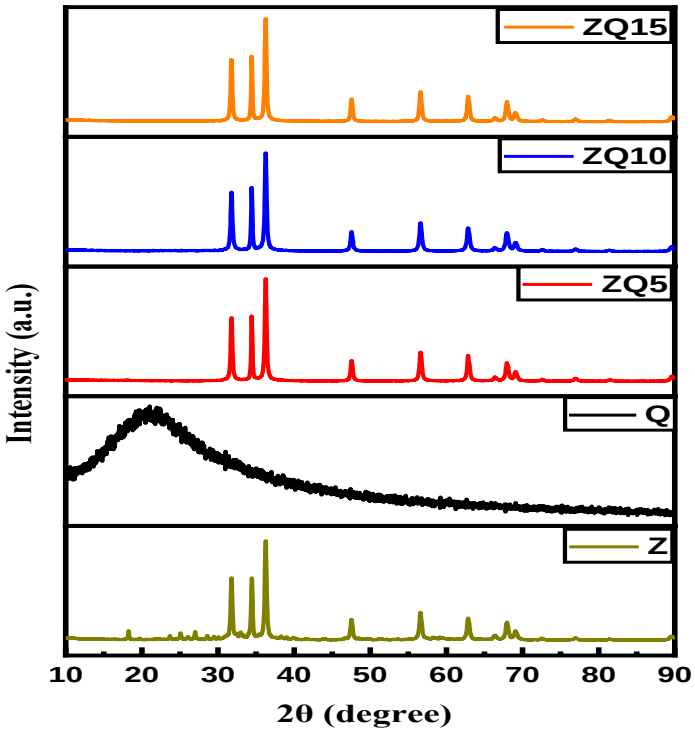

Figure 2. XRD patterns of pure ZnO, CQD's and it's nanocomposites namely ZQ5, ZQ10 and ZQ15.

At 2θ values of 31.73°, 34.5°, 36.22°, 47.50°, 56.9°, and 62.85°, the pure ZnO sample's diffraction pattern showed distinctive peaks that corresponded to the (100), (002), (101), (102), (110), and (103) planes, respectively. The excellent crystallinity and phase purity of ZnO are confirmed by these peaks, which are compatible with its hexagonal wurtzite phase [30]. In line with earlier research, a significant diffraction hump was seen for the CQD's (also known as Q) at about 2θ = 21.02°, suggesting that they are amorphous [32]. The principal peaks linked to ZnO did not alter during the creation of the ZnO-CQD's nanocomposites, exhibiting only slight positional variations. Because of their disorganized, amorphous nature or very low concentration, it is noteworthy that no clear peaks relating to CQD's were found [33]. These findings imply that the crystallographic structure of the host material is not considerably altered by the addition of CQD's to the ZnO matrix. Figure 2. shows the XRD profiles of each sample, which amply demonstrate the structural coherence of ZnO in the composite.

3.2.2. XPS studies

The ZnO-CQD's composite's XPS study is shown in Figure 3. The survey spectrum verifies that the substance contains the elements zinc (Zn), oxygen (O), and carbon (C), as seen in Figure 3a. Two strong peaks in the Zn 2p spectra are shown in Figure 3c. at binding energies of 1043.74 eV and 1020.52 eV, respectively. These correspond to Zn $2p_{1/2}$ and Zn $2p_{3/2}$.

Two peaks at 529.70 eV and 531.25 eV in the composite's high-resolution O 1s spectra are ascribed to Zn–O and C–O bonds, respectively. The commercial ZnO sample, on the other hand, has O 1s peaks at 529.61 eV and 531.31 eV, which suggest the presence of surface hydroxyl groups and Zn–O bonding. These modifications and the FTIR data point to a reaction between the carboxyl groups from CQD's and the hydroxyl groups on the ZnO surface. As shown in Figure 3b., this interaction most likely results in the creation of new C–O bonds and the decrease or removal of hydroxyl signals.

Furthermore, a peak at 284.76 eV in the C 1s spectrum shown in Figure 3d. of the composite is associated with C–C bonds in CQDs. C–O and C=C bonds are linked to peaks at 284.65 eV and 287.05 eV, respectively. The successful incorporation of CQD's into the ZnO structure, resulting in a well-integrated composite, is confirmed by these spectral properties [34].

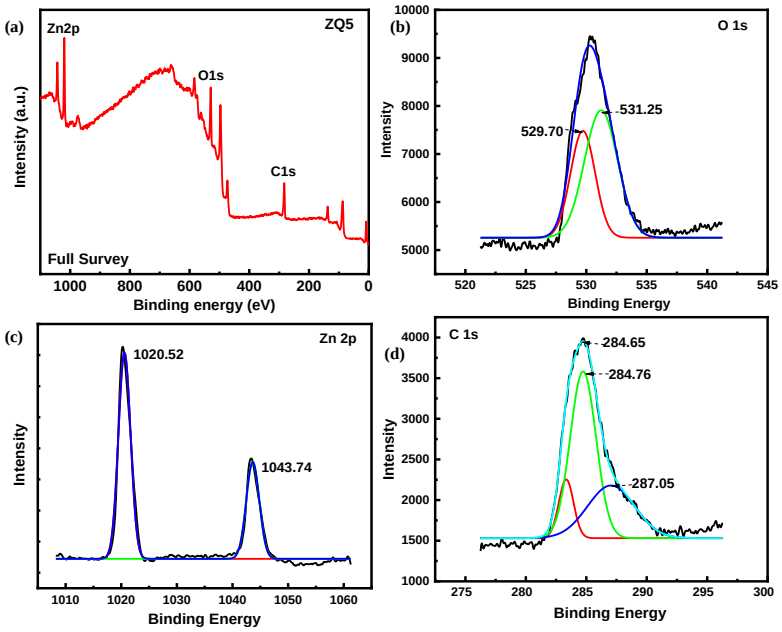

Figure 3. (a) XPS for the full spectrum of ZQ5 (b) Spectrum of O 1s (c) Spectrum of Zn 2p (d) Spectrum of C 1s

3.2.3. Photoluminescence studies

The PL spectra of Zinc Oxide (Z), Carbon Quantum Dots (Q), and their composites (ZQ5, ZQ10, ZQ15) are presented in Figure 4. The pristine Q exhibit a strong and sharp emission peak centered around 565 nm, attributed to the excitonic recombination within the quantum dots. In contrast, pure Z shows a significantly lower emission intensity, indicating its limited radiative recombination efficiency in the visible region.

Upon incorporation of Q into the Z matrix to form ZQ composites, the emission intensity varies with Q loading. The ZQ5 and ZQ10 composites show enhanced emission compared to pure Z, with ZQ10 demonstrating the most notable enhancement among the composites. This enhancement suggests efficient energy transfer from Z to Q and improved radiative recombination. However, at higher loading (ZQ15), a slight reduction in intensity is observed, possibly due to aggregation or quenching effects that can arise from excess Q content.

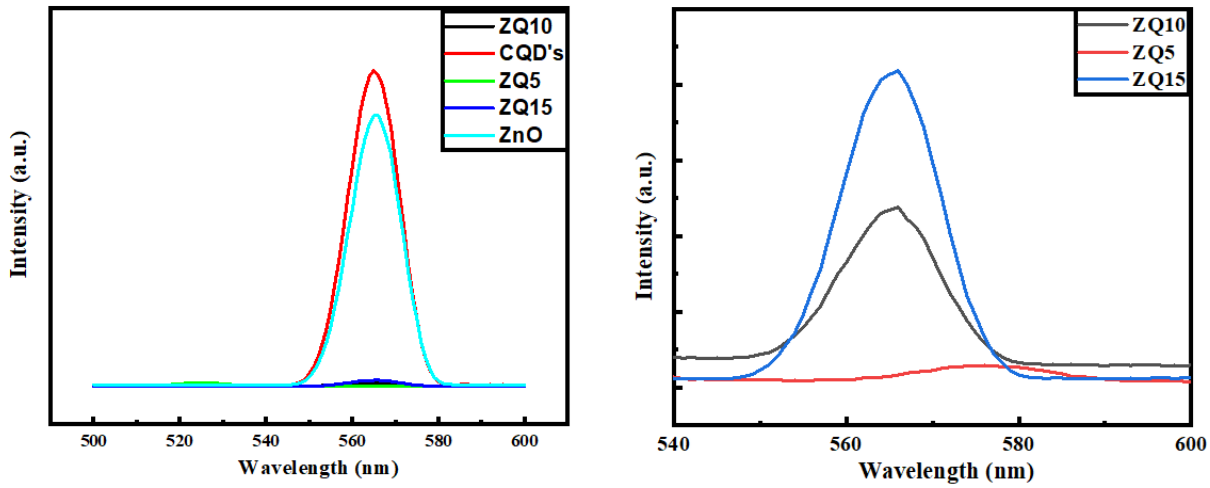

Figure 4. PL spectra of Z, Q, ZQ5, ZQ10, ZQ15.

3.2.4. Surface Properties

The synthesized nanocomposites' specific surface area was measured in order to determine their textural characteristics. The nitrogen adsorption-desorption isotherms are shown in Figure 5. and they exhibit clear H1 hysteresis loops and type IV Langmuir behavior. Mesoporous structures with well-organized pore networks are indicated by these loops, which are seen in both the composite materials and their separate constituents.

Using the Barrett-Joyner-Halenda (BJH) approach, which is also shown in Figure 6., the pore size distribution was examined. Table 2 provides a comparative overview of the pore volume and surface area. Even though clean Z has a significant surface area and pore volume, the nanocomposites show even higher values, indicating that porosity and surface properties are improved by the incorporation of Q.

With varied composite formulations, a progressive rise in surface area was seen across the samples: ZQ5 recorded 11.353, ZQ10 recorded 8.9343 m^2/g, and ZQ15 achieved the highest value at 14.582 m^2/g. By increasing the pollutant adsorption capacity and offering a greater density of reactive sites necessary for catalytic activities, but although ZQ5 shows the maximum result in its enhanced photocatalytic activity due to the blockage of some active sites by the incorporation of Q [35].

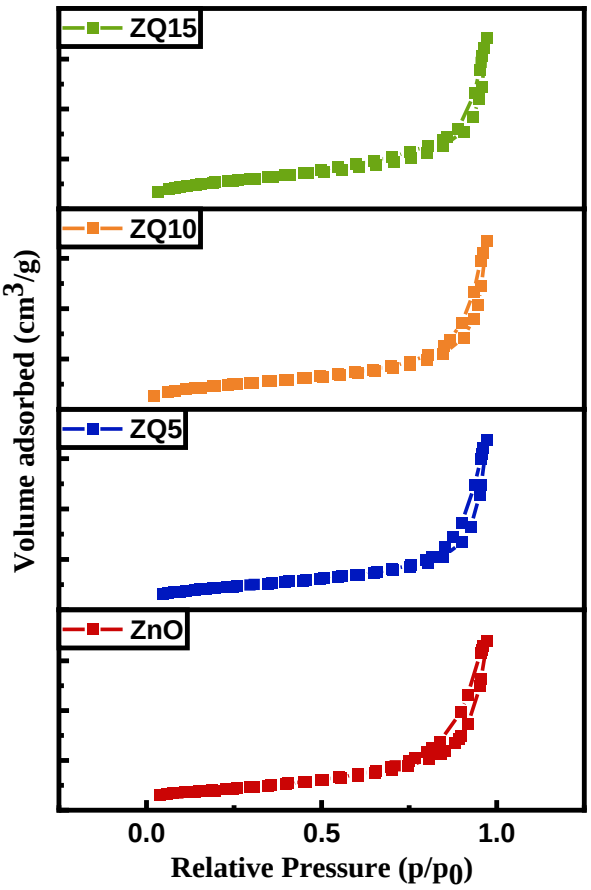

Figure 5. BET isotherms

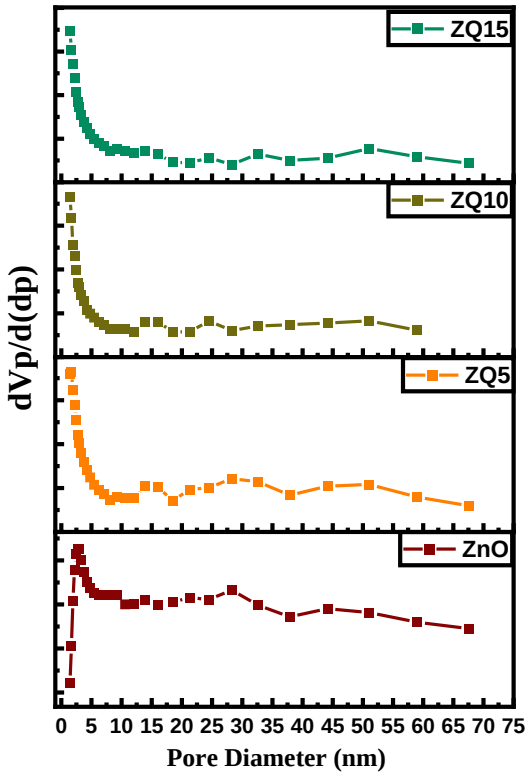

Figure 6. BJH plot to determine the pore size of the synthesized photocatalysts

Table 2. Surface characteristics of the synthesized photocatalysts

Catalyst	Surface area (m^2/g)	Average Pore Size (nm)	Total Pore Volume (cm^3/gm)
Z	12.469	14.303	0.044
ZQ5	11.353	12.689	0.036
ZQ10	8.9343	12.031	0.0269
ZQ15	14.582	10.761	0.0369

3.2.5. Morphological Characterization

The structural properties of the produced materials—Z, Q, and the ZQ5 composite—were systematically examined using Field Emission Scanning Electron Microscopy (FE-SEM). These

related FE-SEM micrographs are shown in Figure 7(a–c). The unique nano-flower-like architecture of the Z sample was in line with morphologies that had been previously documented [30]. The Q component, on the other hand, was thought to have a nano-spherical form; however, because of resolution constraints, these characteristics were not easily discernible in the FE-SEM pictures. High-Resolution Transmission Electron Microscopy (HRTEM) analysis was performed to provide further information shown in the Figure 7 h, j. The HRTEM pictures validated the successful creation of the ZQ5 heterojunction nanocomposite by confirming that the Q particles were uniformly attached onto the flower-like surface of Z. By introducing a high density of active sites, this hierarchical structure greatly expands the surface area and improves photocatalytic performance by improving pollutant adsorption and degradation.

Additionally, the HRTEM images' lattice fringe analysis Figure 7h, j. showed clear d-spacing values that matched the crystallographic planes connected to angles at 34.5°, 36.22°, 47.504°, 56.9°, 62.85°, and 21.02°. The ZQ5 nanocomposite's crystalline nature and phase purity are confirmed by these interplanar distances, which closely match the distinctive diffraction peaks seen in the XRD pattern.

Energy Dispersive X-ray Spectroscopy (EDS) was used to determine the elemental composition Figure 7i, and the results verified that the synthesized material contained carbon (C), nitrogen (N), zinc (Zn), and oxygen (O). Furthermore, the even distribution of each component element throughout the nanocomposite was confirmed by elemental mapping represented in Figure 7d–g. In order to promote effective charge transfer and raise the total photocatalytic activity, this uniformity is essential. The creation of an efficient heterojunction structure, which is necessary for high-efficiency photocatalysis, is further highlighted by the uniform dispersion of Q onto the Z matrix.

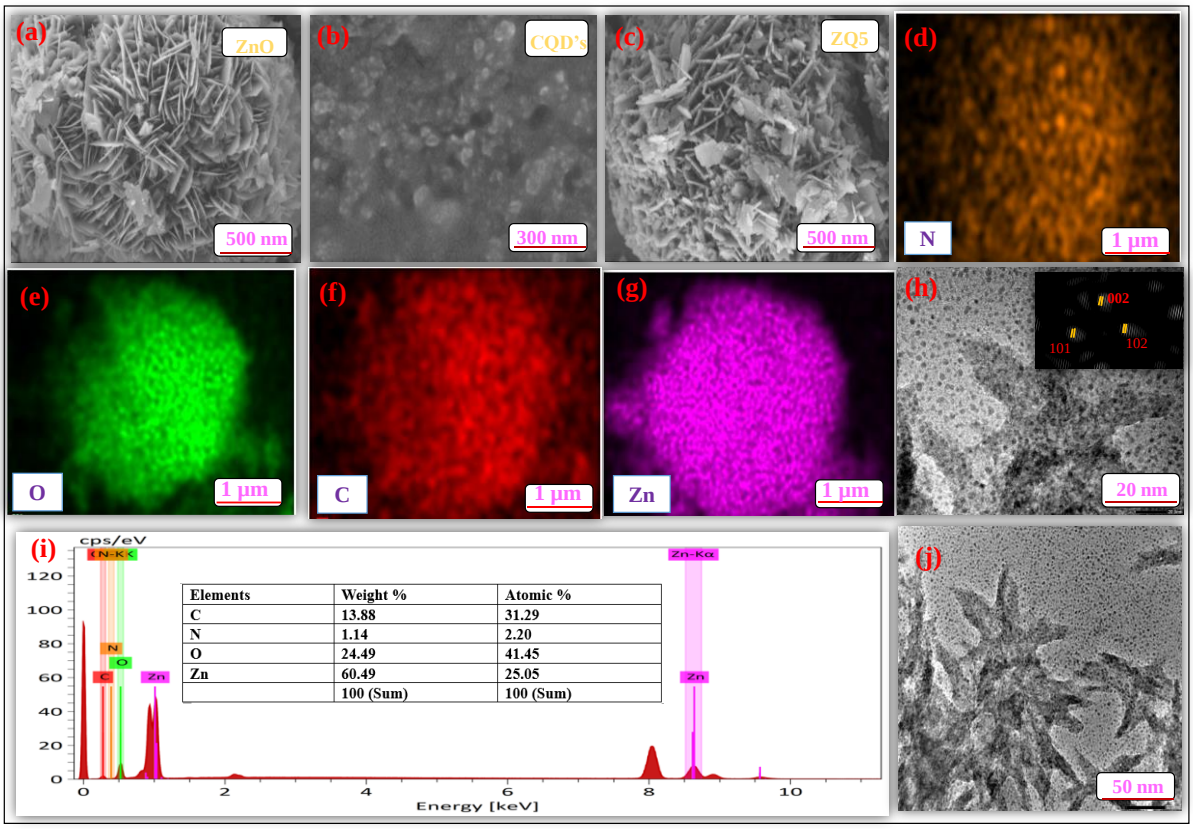

Elements	Weight %	Atomic %
C	13.88	31.29
N	1.14	2.20
O	24.49	41.45
Zn	60.49	25.05
	100 (Sum)	100 (Sum)

Figure 7. FE-SEM Images of (a) Z, (b) Q, (c) ZQ5 (d-g) Elemental mapping of the ZQ5 nanocomposite, (h,j) HR-TEM images of ZQ5 nanocomposite (i) EDS spectrum of the ZQ5 nanocomposite with its corresponding FE-SEM image.

3.2.6. UV-DRS Spectra

A material's ability to absorb light has a significant impact on its photocatalytic efficiency. UV–visible diffuse reflectance spectroscopy (UV-DRS) was used to assess the optical absorption characteristics of the synthesized samples Z, Q, and the nanocomposites ZQ5, ZQ10, and ZQ15. The UV–vis absorption spectra demonstrate in Figure 8a. shows that the pure Z material primarily absorbs light in the ultraviolet spectrum, more precisely in the wavelength range of 250–400 nm. On the other hand, the absorption profile is drastically changed when Q is added to the Z matrix. The absorption margins of the ZQ nanocomposites were widened and extended into the visible spectrum. This improvement is explained by Q's photosensitizing action, which strengthens the material's absorption of visible light.

Additionally, a noticeable color shift was seen in the materials as the Q content increased, moving from the pure Z's initial white look to increasingly deeper tones in the ZQ5, ZQ10, and ZQ15 composites. This visual alteration shows enhanced light harvesting in the visible region, which is crucial for effective photocatalytic activity under solar irradiation, and further supports the successful integration of Q into the Z structure

To determine the bandgap energies of these materials, Tauc's equation: -

$$(\alpha h\nu)^{1/n} = A(h\nu - Eg) \quad (1)$$

was employed, where hν is the photon energy, Eg represents the optical bandgap, α is the absorption coefficient, A is a proportionality constant, and n=1/2 corresponds to the direct allowed transition type characteristic of the studied materials.

The estimation of the optical bandgap energies was made possible by extrapolating the linear section of the curves by graphing $(\alpha h\nu)$ 1/ 2 versus $h\nu$, as illustrated in Figure 8b. Pure Z has a predicted bandgap of 3.10 eV, Q 2.95 eV, and the ZQ5, ZQ10, and ZQ15 composites 2.93 eV, 3.07 eV, and 3.05 eV, respectively. These minor bandgap differences between the composites show the impact of Q integration; ZQ5 shows the largest decrease, indicating a better band alignment and improved visible-light consumption. Under visible light irradiation, this bandgap narrowing improves light absorption and is anticipated to increase the composite materials' photocatalytic efficiency.

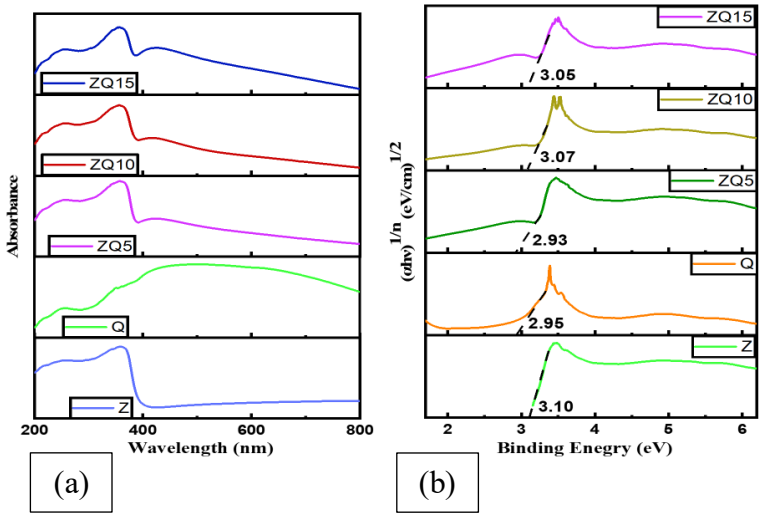

Figure 8. (a) The band gap energies of Z, Q, ZQ5, ZQ10, and ZQ15, and (b) UV- Visible DRS absorption spectra

3.2.7. FTIR analysis

Fourier Transform Infrared (FTIR) spectroscopy was employed to identify the functional groups present in the synthesized materials (Z, Q, ZQ5, ZQ10, ZQ15). The spectra were recorded within the range of 4000–400 cm^{-1}, as illustrated in Figure 9.

In the FTIR spectrum of Z, a broad peak at approximately 3475 cm^{-1} was attributed to the stretching vibrations of –OH groups, indicating the presence of surface-bound water or hydroxyl functionalities. A peak at 2962 cm^{-1} was assigned to the stretching vibrations of methylene $–CH_2$ groups. The appearance of a distinct peak around 1633 cm^{-1} confirmed the presence of C=O functionalities. The band at 752 cm^{-1} corresponded to H–O–H bending, suggesting molecular water within the crystal lattice, while another band at 644 cm^{-1} was linked to lattice deformation. Additional peaks at 1507, 1382, and 845 cm^{-1} were attributed to CO_3^{2-} vibrational modes, and the peak at 1560 cm^{-1} reflected symmetric C=O stretching, in agreement with literature data [30].

The FTIR spectrum of Q displayed broad absorption bands between 3135 and 3576 cm^{-1}, which were characteristic of carboxylic acid O–H stretching. An absorption band at 1588 cm^{-1} was associated with N–H bending vibrations, further corroborated by a smaller peak near 2351 cm^{-1}. A sharp peak at 1167 cm^{-1} indicated the presence of C–O stretching, confirming oxygen-containing functional groups in the material [31].

In the spectra of the ZQ nanocomposites, characteristic bands from both Z and Q were retained, though with minor shifts in their positions. These shifts suggest chemical interactions between Z and Q components and support the successful formation of the composite materials. The preservation of functional group signatures across all nanocomposites indicates structural integrity, while the spectral changes provide evidence of effective bonding and composite synthesis.

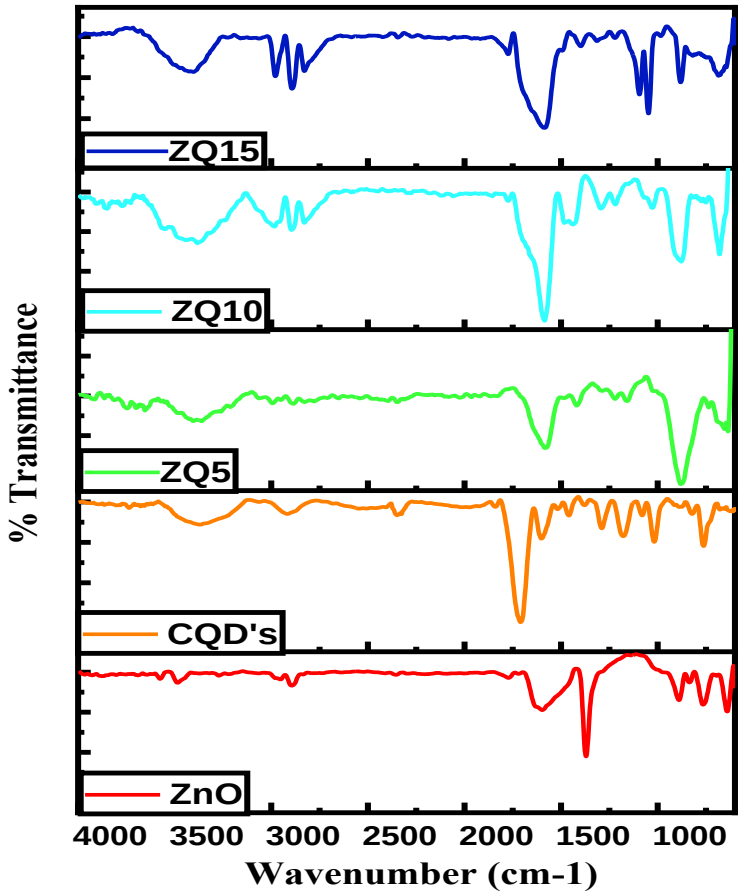

Figure 9. FTIR spectra of Z, Q, ZQ5, ZQ10, ZQ15.

3.2.8. Photocatalytic activity

MB degradation under various irradiation conditions measured the ZQ5 nanocomposite's photocatalytic efficiency. At the Thapar Institute of Engineering & Technology in Patiala, India, the trials were conducted in a subtropical environment with open sunlight. During the experiments, the average intensity of solar irradiation was measured with a LICOR pyranometer and found to be around 850 W/m². An almost 100 W/m² light intensity was produced by a 45 W Philips compact fluorescent bulb, which was used to replicate visible light conditions. In order to achieve ultraviolet irradiation, a 100 W mercury lamp with a light flux density between 66 and 68 W/m² was used to emit light at 365 nm.

For the purpose of ensuring data reproducibility and dependability, every photocatalytic experiment was carried out in triplicate. After analysis, the data were displayed with error bars that showed a margin of error of ±5%. Throughout the photocatalytic process, a UV-visible spectrophotometer was used to measure absorbance at the maximum wavelength (λmax) of 660 nm at regular intervals to track the concentration of MB. A precise evaluation of the ZQ5 nanocomposite's photocatalytic performance was made possible by the subsequent calculation of the degradation efficiency of MB using a standard formula (in equation no 2) based on the change in absorbance over time.

$$\%\, Degradation = \frac{A_t - A_0}{A_t} \times 100 \quad (2)$$

The ZQ5 nanocomposite's photocatalytic performance was systematically assessed by measuring how well MB degraded in the presence of sunlight. Using a typical photometric approach, the degradation percentage was determined by comparing the absorbance at time t (A_t) with the initial absorbance (A_0). For the studies, a 10 mL solution of 10 ppm MB was utilized. To achieve adsorption–desorption equilibrium, the solution was agitated in the dark for 60 minutes before being exposed to light. Using ZQ5, the maximum degradation efficiency was 97.2% after 60 minutes of exposure to natural sunshine. Reaction kinetics were first studied at a catalyst concentration of 0.1 g/L; Figure 10a. displays the matching degradation curve. ZQ5's higher performance was confirmed by comparative investigations utilizing Z, Q, ZQ10, ZQ15, and commercial TiO_2 (P25). A pseudo-first-order kinetic model was used to determine the apparent rate constant (k), which allowed for a direct comparison of photocatalytic activity in all materials. The impact of different ZQ5 concentrations (0.1–0.6 g/L) was also investigated in order to maximize catalyst loading. The results showed that there was no discernible increase in degrading efficiency when the catalyst amount was increased above 0.1 g/L. The system consistently achieved ~97% degradation in 60 minutes at 0.1 g/L, making it the most affordable and efficient loading method. This concentration provided the best active surface area without causing significant scattering or light shielding, as illustrated in Figure 10b., making it the perfect dosage for additional research. We computed the rate constant, (k) using the equation 3:

$$\ln \frac{C}{C_0} = -kt \quad (3)$$

The initial dye concentration (C_0), the concentration at time t (C), and the apparent rate constant

(k) were used to examine the photocatalytic degradation kinetics. As shown in Figure 10a., the degradation data showed that the reaction followed a pseudo-first-order kinetic model. The ZQ5 nanocomposite demonstrated the greatest rate constant of 0.047 min^{-1} among the materials studied, demonstrating its enhanced photocatalytic efficiency. In contrast, the rate constants for the bare components Z and Q were 0.015 min^{-1} and 0.0092 min^{-1}, respectively. Additionally, the ZQ10 and ZQ15 composites performed worse, with rate constants of 0.019 and 0.017 min^{-1}, respectively and for the commercially available TiO_2-P25 whose rate constant is 0.0082 min^{-1}. The degree of synergistic impact in the composites was evaluated by computing the synergy factor (R) using the equation 4:

$$R = \frac{K_{ZQ}}{K_Z + K_Q} \tag{4}$$

Because of its higher photocatalytic degradation efficiency, the ZQ5 binary nanocomposite showed the highest synergy factor among all examined samples. In comparison to the separate components, this result demonstrates that the ZQ5 composite's ideal ratio of Z and Q integration produces a synergistic interaction that improves charge separation and light absorption, hence greatly increasing photocatalytic activity. The synergy factor analysis makes it abundantly evident that Z and Q combined impact in the composite is more potent than the sum of their individual accomplishments.

For comparison analysis, Table 3 summarizes the computed rate constants and associated synergy factors for all photocatalysts: Z, Q, ZQ5, ZQ10, ZQ15, and commercial TiO_2-P25. These findings confirm the ZQ5 composite's potential as a highly active and well-optimized photocatalyst for solar-driven environmental remediation and further highlight its exceptional efficiency.

Table 3. The synergy factors and degradation rate constants attained by photo-catalytic MB elimination

Material	Rate Constant (min^{-1})	Synergy Factor (R)
TiO_2-P25	0.0082	----------
ZnO	0.015	----------
CQD's	0.0092	----------
ZQ5	0.047	2.02
ZQ10	0.019	0.81
ZQ15	0.017	0.73

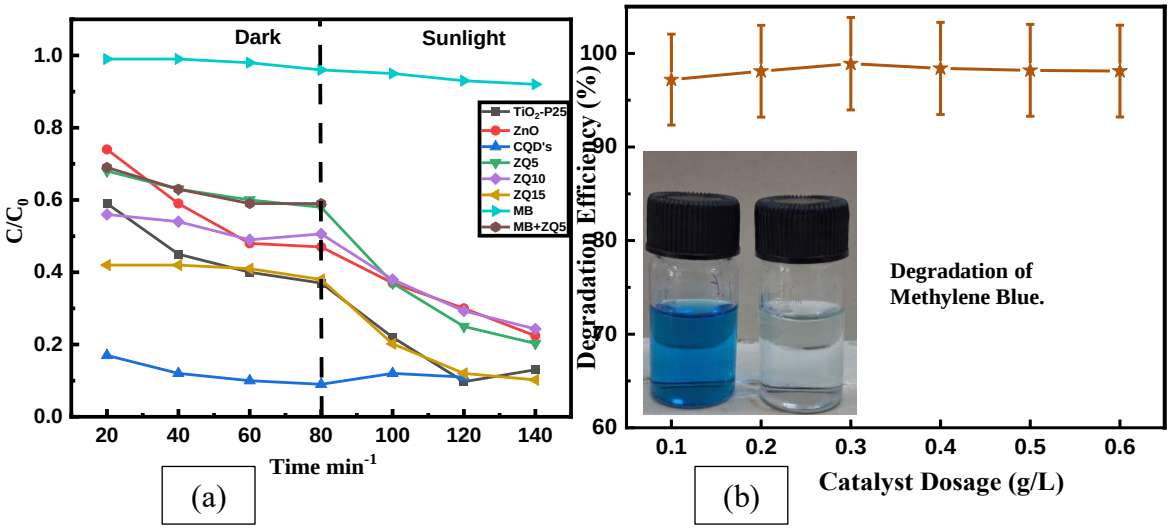

Figure 10. (a) Degradation Kinetics of MB under controlled conditions (0.1g/l catalyst, 10 ml dye solution, pH is near about 7.8 and 60 minutes of sunlight irradiation) (b) Impact of ZQ5 photocatalyst concentration.

3.2.9. Effect of Light Sources

Under ideal circumstances, a comparative analysis was carried out to assess the ZQ5 nanocomposite's photocatalytic efficiency under a range of light sources, including visible light,

UV light, and sunlight. The degradation efficiency of MB under UV irradiation was 62.1%, whereas the degradation efficiency under visible light irradiation was 38.8%. On the other hand, exposure to natural sunshine greatly improved the photocatalytic function, resulting in an 89.2% degradation efficiency. Due to its higher energy intensity and wider spectrum range than artificial light sources, these results highlight the superior role of solar radiation in activating the ZQ5 photocatalyst. The improved performance in direct sunlight further demonstrates ZQ5's promise for practical, environmentally friendly uses. Figure 11. provides a graphic representation of the comparative degradation behavior under various light circumstances, demonstrating the photocatalytic process's dominant effectiveness when driven by natural sunshine.

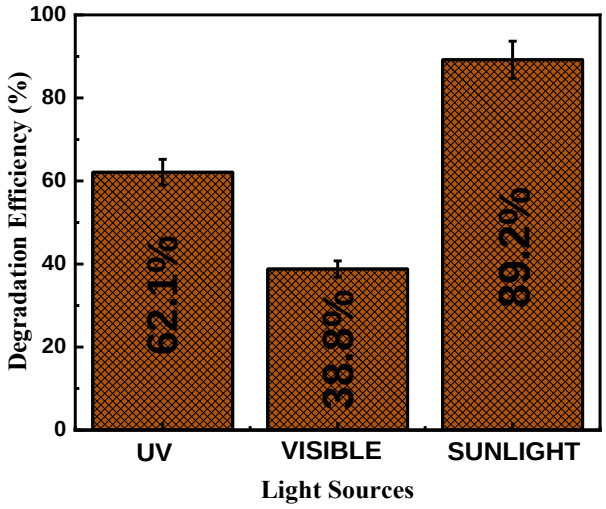

Figure 11. Variations in MB degradation using a 13GS photocatalyst brought on by varying light intensities.

3.2.10. Effect of solution pH

The photocatalyst's surface charge and interaction with pollutant molecules are significantly impacted by the dye solution's pH. A crucial stage of photocatalytic degradation, dye adsorption on the catalyst surface, is directly impacted by these variables. Consequently, enhancing photocatalytic performance requires pH optimization [36]. As the dye solution's pH changed from acidic to alkaline, the ZQ5 nanocomposite's photocatalytic degradation efficiency increased significantly, reaching over 95% between pH 8 and 12, as seen in Figure 12a. As illustrated in Figure 12b., the material's point of zero charge (pzc), which was found to be roughly 7.8, is

strongly linked to this enhanced performance. The electrostatic interaction between the catalyst and the cationic MB dye molecules is increased as the pH rises over this threshold because the photocatalyst's surface becomes negatively charged. A crucial first step in starting photocatalytic reactions, this enhanced attraction facilitates more efficient dye adsorption onto the catalyst surface. Moreover, hydroxide ions (OH^-) are more abundant in alkaline circumstances and are easily transformed into reactive hydroxyl radicals ($^{\bullet}OH$) when exposed to light. During photocatalysis, these radicals are essential for the breakdown of organic contaminants. The increased degradation efficiency seen at higher pH levels is mostly due to the combination effects of improved dye adsorption and enhanced radical production under alkaline conditions.

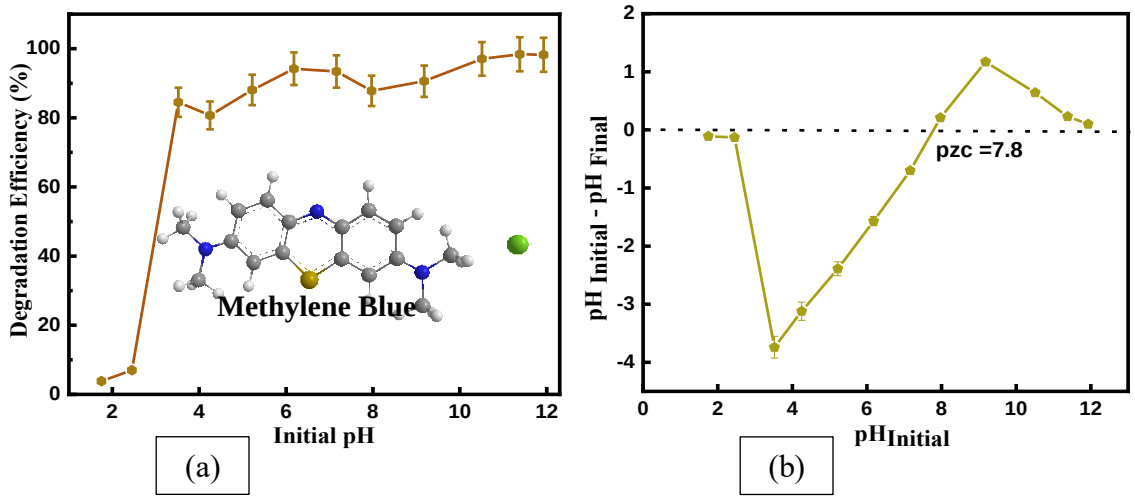

Figure 12. (a) Effect of pH on MB degradation (b) pzc value of ZQ5 nanocomposite.

3.2.11. Reusability studies

For a photocatalyst to be used practically, its long-term durability and reusability must be assessed in addition to its photocatalytic performance. A number of recycling tests were conducted to investigate the ZQ5 photocatalyst's photostability and recyclability. The degradation of methylene blue (MB) under uniform experimental circumstances over several cycles was the main focus of these studies. Prior to being used again, the ZQ5 catalyst was centrifuged, cleaned, and dried after every photocatalytic run.

Even after six consecutive cycles, ZQ5 maintained a high degradation efficiency of 81%, indicating great reusability, as seen in Figure 13a. Minor catalyst losses during recovery and the buildup of leftover intermediate products on the catalyst surface, which could partially choke

active sites, are probably the causes of the slight decline in performance from the initial 98%. As shown in Figure 13c, post-cycling examination was carried out utilizing X-ray diffraction (XRD) to further examine the catalyst's structural stability. The crystal structure was confirmed to have been preserved after repeated use by the XRD patterns, which showed no discernible changes in peak locations or intensities or the emergence of any new peaks. Furthermore, field emission scanning electron microscopy (FE-SEM) pictures (Figure 13d.) verified that the ZQ5 composite's surface shape did not change during the photocatalytic process.

Together, these findings highlight the ZQ5 nanocomposite's exceptional stability, structural integrity, and reusability, highlighting its potential for useful and sustainable photocatalytic applications.

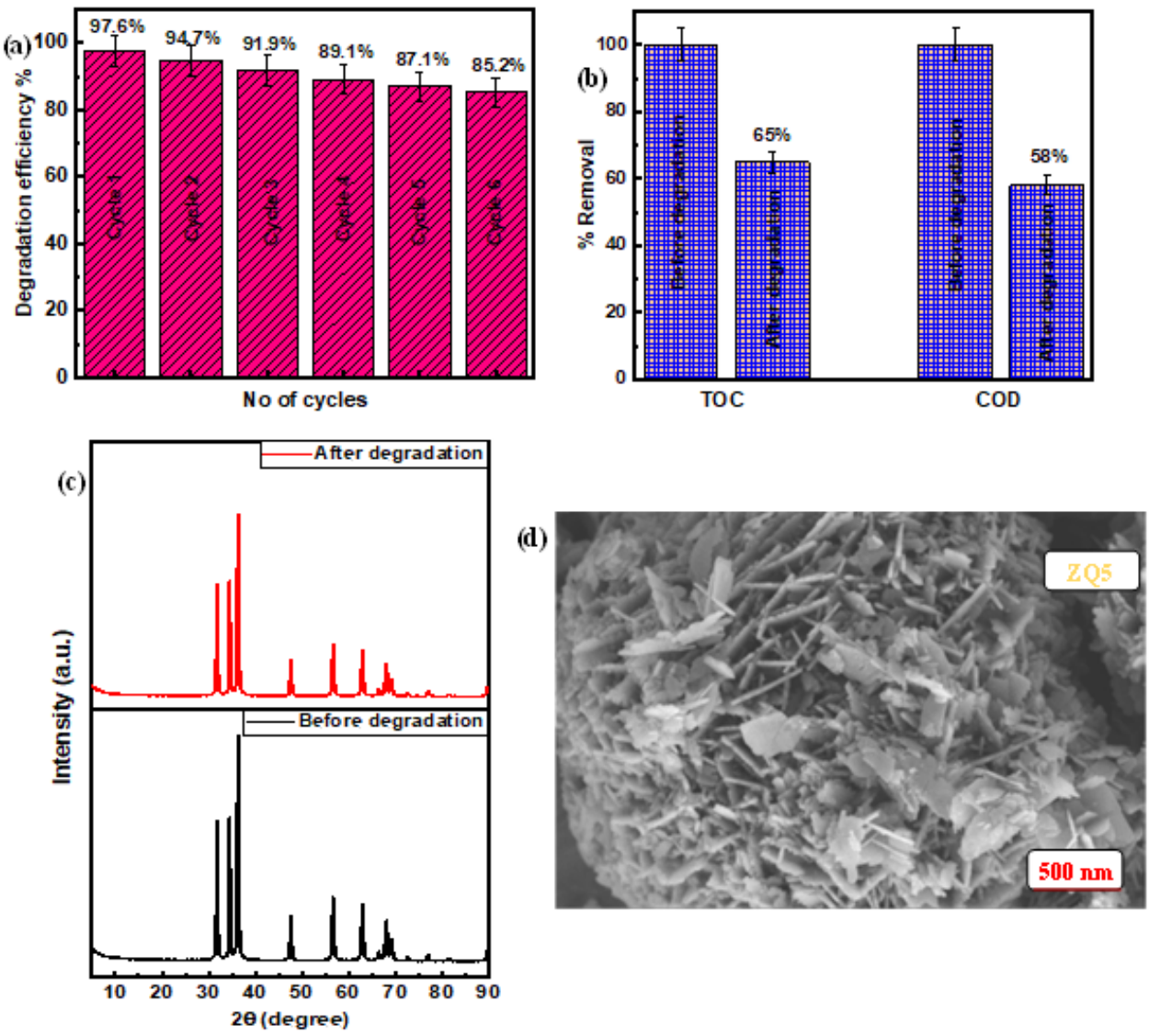

Figure 13. (a) Reusability Graph (b) Analysis of TOC and COD levels before and after degradation (c) XRD spectra of ZQ5 nanocomposite before and after degradation (d) FE-SEM of ZQ5 nanocomposite after degradation

3.2.12. Mineralization studies

Using clean water as the reference standard, titrimetric techniques were used to measure Total Organic Carbon (TOC) and Chemical Oxygen Demand (COD) in order to evaluate the mineralization capabilities of the ZQ5 nanocomposite. Equations (5) and (6) were used to get the percentage decreases in TOC and COD, respectively:

$$\%TOC = \frac{TOC_i - TOC_f}{TOC_i} \times 100 \quad (5)$$

$$\%COD = \frac{COD_i - COD_f}{COD_i} \times 100 \quad (6)$$

TOC_i and TOC_f indicate the starting and ending TOC values in this case, whereas COD_i and COD_f stand for the corresponding COD values. According to the preliminary readings, the MB dye solution had a high organic content. Significant reductions of 89.5% in TOC and 25% in COD were noted following 60 minutes of sun irradiation as shown in Figure 13b. Despite considerable degradation, the relatively smaller decrease in TOC is probably caused by the intermediate organic species that are formed during the photocatalytic process [37]. The full mineralization of MB into carbon dioxide and other simpler, non-toxic byproducts depends on these intermediates. The simulated results, as displayed, reveal near-complete mineralization with low leftover intermediates remaining for further breakdown, notwithstanding the ethical limits that prevented testing of actual pharmaceutical or clinical wastewater samples.

3.2.13. Scavenger effect and a potential charge transfer pathway

The interaction between photogenerated charge carriers—holes in the valence band (VB) and electrons in the conduction band (CB)—and the reactive oxygen species they produce, like superoxide ($^{\bullet}O_2^-$) and hydroxyl ($^{\bullet}OH$) radicals, is essential to the photocatalytic degradation process. Together, these species attack and break down complex organic contaminants, eventually converting them into less dangerous or mineralized forms [11]. Using selective chemical agents, scavenger research was carried out to determine the main reactive species in charge of the photocatalytic degradation process. The reaction system was supplemented with specific scavengers, including benzoquinone (BQ) to scavenge superoxide radicals ($^{\bullet}O_2^-$), methanol to capture photogenerated holes (h^+), dimethyl sulfoxide (DMSO) to trap electrons (e^-), and isopropyl alcohol (IPA) to quench hydroxyl radicals ($^{\bullet}OH$). A better knowledge of their functions was made possible by the selective inhibition of each scavenger's associated species' activity. Interestingly, BQ's involvement in the breakdown pathway is confirmed when it combines with the superoxide radical ($^{\bullet}O_2^-$), a strong reducing agent, to generate hydroquinone [38]. The scavenger study's use of DMSO emphasizes how important $^{\bullet}OH$ are to the photocatalytic breakdown process. Because of the unpaired electrons on the oxygen atoms, which form hydrogen bonds with the hydrogen in hydroxyl radicals, DMSO works by promoting electron

transfer. This interaction emphasizes how important •OH radicals are to the degradation process [39]. When no scavenger was present, the breakdown of MB peaked at 98%, indicating the ZQ5 composite's high efficiency. However, a discernible decrease in the rate of photocatalytic degradation was noted upon the addition of scavengers to the reaction system. The addition of methanol had a notable effect, as illustrated in Figure 14., underscoring the key function of h^+ in the photocatalytic process. Although they had a less noticeable effect, DMSO and IPA significantly decreased the degradation efficiency, indicating that e^- and •OH are also crucial, albeit secondary, components of the overall degradation mechanism. The proposed photocatalytic degradation mechanism is illustrated in Scheme 2. The key reaction stages involved in the photocatalytic process are outlined in Equations 7 to 11, which describe the interactions between the photocatalyst and the contaminants, as well as the formation of reactive species responsible for the degradation process.

$$\mathbf{ZnO/CQD + hv \rightarrow e^- + h^+} \quad \mathbf{(7)}$$

$$\mathbf{e^-_{CB} + O2 \rightarrow O2^{\cdot -}} \quad \mathbf{(8)}$$

$$\mathbf{O2^{\cdot -} + H2O \rightarrow HOO^{\cdot} + OH^{\cdot}} \quad \mathbf{(9)}$$

$$\mathbf{h^+_{VB} + OH^- \rightarrow OH^{\cdot}} \quad \mathbf{(10)}$$

$$\mathbf{OH^{\cdot}/h^+ + Pollutant \rightarrow Degraded\ products} \quad \mathbf{(11)}$$

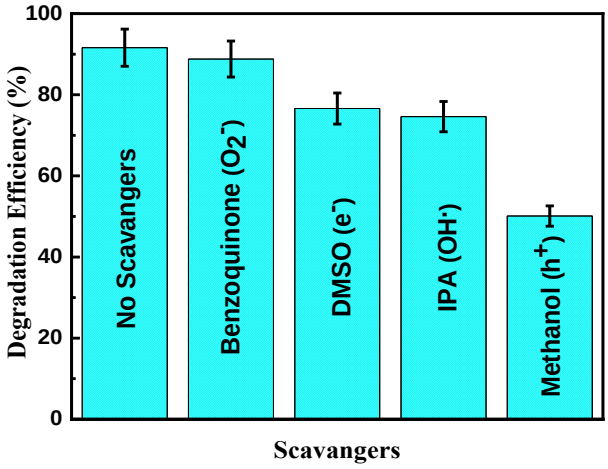

Figure 14. Different scavengers' effects on MB degradation

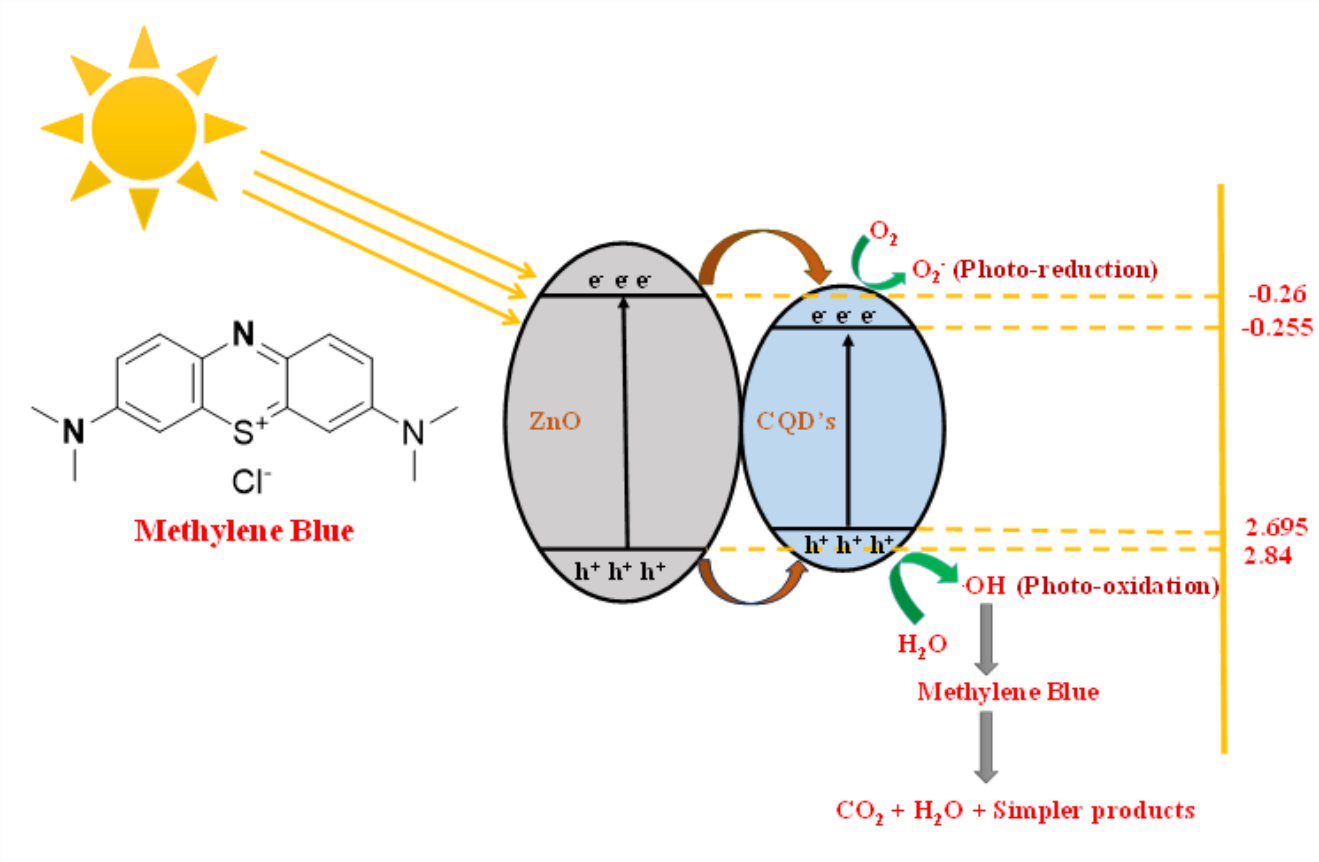

Scheme 2. The suggested pathway for the ZQ5 nanocomposite's photodecomposition of pollutants

3.2.14. LC-MS

MB breakdown happens through a number of processes, according to an LC-MS analysis. MB (m/z = 284) is hydroxylated and demethylated in Pathway 1 before to full mineralization, resulting in intermediates at m/z = 318, 340, and 396 that further break down into smaller fragments such m/z = 109 and 130 [40]. Pathway 2 employs hydrodynamic cavitation to produce polyhydroxylated products at m/z = 350 and 366, which are fueled by hydroxyl radicals that promote ring opening and molecular breakage [41]. MB is converted via one of the two approaches outlined in Pathways 3 and 4 to m/z = 215, m/z = 158, and m/z = 74. The alternative path indicates total ring disintegration and demethylation, passing through m/z = 136, 137, and 109 before reaching the identical terminal product at m/z = 74 [42]. These findings demonstrate how important hydroxyl radicals are in converting MB into safer, less complicated compounds which is represented in Scheme 3.

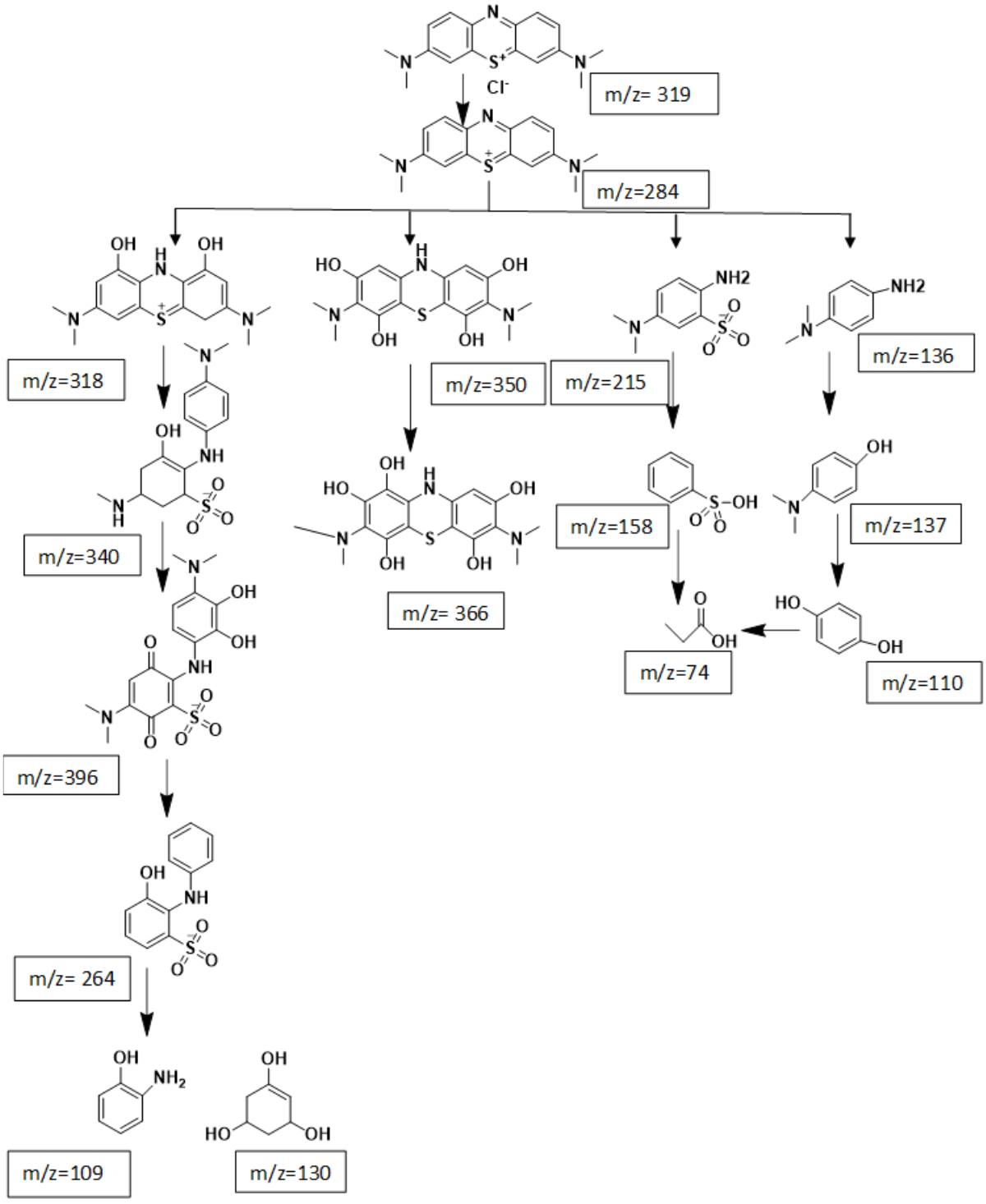

Scheme 3. Potential photocatalytic reaction route of MB using ZQ5 photocatalyst.

CHAPTER 4 – CONCLUSION AND FUTURE SCOPE

A hydrothermal technique was successfully used to create ZnO-CQD's heterojunction photocatalysts in different ratios. Through XRD, FE-SEM, EDS, XPS, UV-DRS, and BET characterization, the composites' effective synthesis and morphology were verified. Smaller CQD's formed a heterojunction on bigger ZnO nanoflowers, as seen by FE-SEM photos. Because ZQ5 has an ideal band gap and less charge recombination than the other composites, it demonstrated the best photocatalytic degradation efficiency for MB when exposed to natural sunshine. A number of variables, including light source, pH, catalyst dosage, and reusability, affected the photocatalytic performance. According to scavenger tests, the main species causing MB deterioration were holes (h^+). Throughout six cycles, the composite demonstrated outstanding reusability with negligible performance degradation. Without changing the catalyst's structure, MB adsorption was verified by XRD and FE-SEM. With notable COD and TOC elimination, the ZQ5 composite performed better than traditional techniques. The effectiveness of the catalyst was further validated by LC-MS analysis, which verified the full mineralization of MB. For solar-powered applications in environmental cleanup, ZnO-CQD's is a particularly promising photocatalyst.

Large-scale industrial wastewater treatment is made possible by these catalysts, which have great potential for effectively combating complex contaminants. They are ideal for a variety of wastewater treatment applications due to their price, usability, and environmental sustainability. These catalysts provide a workable, environmentally responsible way to improve water quality and safeguard the health of the environment by efficiently lowering the accumulation of dangerous pollutants in aquatic habitats.

References

1 S. Dong, J. Feng, M. Fan, Y. Pi, L. Hu, M. Liu, J. Sun and C. Du, *RSC Adv*, 2015, **5**, Ahead of Print.

2 H. Deng, J. Yin, J. Ma, J. Zhou, L. Zhang, L. Gao and T. Jiao, *Appl Surf Sci*, 2020, **543**, 148821.

3 J. Qu and M. Fan, *Crit Rev Environ Sci Technol*, 2010, **40**, 519–560.

4 A. Houas, H. Lachheb, M. Ksibi, E. Elaloui, C. Guillard and J.-M. Herrmann, *Appl Catal B*, 2001, **31**, 145–157.

5 P. Zhang, M. Xiang, H. Liu, C. Yang and S. Deng, *ACS Appl Mater Interfaces*, 2019, **11**, 24027–24036.

6 C. Hou, B. Hu and J. Zhu, *Catalysts*, 2018, **8**, 575.

7 M. Basibuyuk and C. F. Forster, *Process Biochemistry*, 2003, **38**, 1311–1316.

8 G. Zhu, H. Fang, Y. Xiao and A. Hursthouse, *J Fluoresc*, DOI:10.1007/s10895-020-02591-2.

9 E. Alventosa-deLara, S. Barredo-Damas, M. I. Alcaina-Miranda and M. I. Iborra-Clar, *J Hazard Mater*, 2012, **209–210**, 492–500.

10 P. Sethi, S. Barman and S. Basu, *Sep Purif Technol*, 2025, **361**, 131311.

11 A. Kundu, S. Sharma and S. Basu, *Journal of Physics and Chemistry of Solids*, 2021, **154**, 110064.

12 P. Sethi, S. Basu and S. Barman, *New Journal of Chemistry*, DOI:10.1039/D5NJ00556F.

13 T. Hisatomi, J. Kubota and K. Domen, *Chem Soc Rev*, DOI:10.1039/c3cs60378d.

14 N. Roy and A. Roy, *Journal of Materials Science: Materials in Electronics*, DOI:10.1007/s10854-014-1721-9.

15 N. Roy, A. Chowdhury and A. Roy, *J Appl Phys*, 2014, **115**, 223502.

16 N. Roy and A. Roy, *Ceram Int*, 2015, **41**, 4154–4160.

17 N. Roy, A. Chowdhury, T. Paul and A. Roy, *J Nanosci Nanotechnol*, 2016, **16**, 9738–9745.

18 L. K. Adams, D. Y. Lyon and P. J. J. Alvarez, *Water Res*, 2006, **40**, 3527–3532.

19 R. Wang, K.-Q. Lu, Z.-R. Tang and Y.-J. Xu, *J Mater Chem A Mater*, 2017, **5**, 3717–3734.

20 K. A. S. Fernando, S. Sahu, Y. Liu, W. K. Lewis, E. A. Guliants, A. Jafariyan, P. Wang, C. E. Bunker and Y.-P. Sun, *ACS Appl Mater Interfaces*, 2015, **7**, 8363–8376.

21 S. J. Phang and L.-L. Tan, *Catal Sci Technol*, 2019, **9**, 5882–5905.

22

23 Y. Huang, Y. Liang, Y. Rao, D. Zhu, J. Cao, Z. Shen, W. Ho and S. C. Lee, *Environ Sci Technol*, 2017, **51**, 2924–2933.

24 S. Selvaraj, D. S. Patrick, V. S. Manikandan, G. A. Vangari, M. K. Mohan and M. Navaneethan, *Surfaces and Interfaces*, 2024, **51**, 104538.

25 Y. Rati, Y. N. Hendri, R. Waluyo, F. Zendrato, A. S. Rini, R. Marlina, R. Kurniawan and Y. Darma, *Opt Mater (Amst)*, 2023, **135**, 113370.

26 N. A. F. Al-Rawashdeh, O. Allabadi and M. T. Aljarrah, *ACS Omega*, 2020, **5**, 28046–28055.

27 U. A. Rani, L. Y. Ng, C. Y. Ng, E. Mahmoudi, Y.-S. Ng and A. W. Mohammad, *Journal of Water Process Engineering*, 2021, **40**, 101816.

28 Y. Qu, X. Xu, R. Huang, W. Qi, R. Su and Z. He, *Chemical Engineering Journal*, 2020, **382**, 123016.

29 N. C. T. Martins, J. Ângelo, A. V. Girão, T. Trindade, L. Andrade and A. Mendes, *Appl Catal B*, 2016, **193**, 67–74.

30 S. Mohan, M. Vellakkat, A. Aravind and R. .U, *Nano Express*, 2020, **1**, 030028.

31 H. Shabbir, T. Tokarski, D. Ungor and M. Wojnicki, *Materials*, 2021, **14**, 7604.

32 S. U. Islam, U. Latief, J. Ali and Mohd. S. Khan, *Spectrochim Acta A Mol Biomol Spectrosc*, 2024, **304**, 123292.

33 H. Bozetine, Q. Wang, A. Barras, M. Li, T. Hadjersi, S. Szunerits and R. Boukherroub, *J Colloid Interface Sci*, 2016, **465**, 286–294.

34 X.-Y. Jin, W.-Y. Ying, R.-J. Che, P. Xiao, Y.-Q. Zhou, Y. Liu, M.-Y. Liu and S.-P. Chen, *RSC Adv*, 2022, **12**, 23692–23703.

35 A. Mehta, A. Mishra, S. Kainth and S. Basu, *Mater Des*, 2018, **155**, 485–493.

36 A. Kumar, R. Kumar and G. Pandey, *Macromol Symp*, 2018, **379**, 1600192.

37 S. Singla, P. Devi and S. Basu, *Catalysts*, 2023, **13**, 731.

38 S. Singla, S. Sharma and S. Basu, *J Clean Prod*, 2021, **324**, 129290.

39 H. Alamgholiloo, E. Asgari, S. Nazari, A. Sheikhmohammadi, N. Noroozi Pesyan and B. Hashemzadeh, *Sep Purif Technol*, 2022, **300**, 121911.

40 O. Intharaksa, S. Nanan, N. Patdhanagul, T. Panphojan, T. Srikakul, N. Tantisuwichwong, N. Tantisuwichwong and R. Dulyasucharit, *Journal of Physics and Chemistry of Solids*, 2023, **182**, 111577.

41 Y. Cao, G. Wu, Y. Huang and C. Huang, *ACS Omega*, 2024, **9**, 39997–40009.

42 J. Lin, Z. Luo, J. Liu and P. Li, *Mater Sci Semicond Process*, 2018, **87**, 24–31.

Hitesh MSc Thesis

ORIGINALITY REPORT

12%	6%	8%	1%
SIMILARITY INDEX	INTERNET SOURCES	PUBLICATIONS	STUDENT PAPERS

PRIMARY SOURCES

1	Bhavika Garg, Pritam Hait, Soumen Basu. "Unlocking solar energy's potential: Dual photocatalytic activities of g-C3N4/Sb2S3 for hydrogen evolution and tetracycline degradation in sunlight", Journal of Environmental Management, 2024 Publication	3%
2	Pritam Hait, Rajeev Mehta, Soumen Basu. " Design and synthesis of PANI/GO/MoS nanocomposites oxidative polymerization for efficient photocatalytic applications: organic pollutant degradation and hydrogen generation ", Materials Advances, 2025 Publication	1%
3	www.science.gov Internet Source	1%
4	www.mdpi.com Internet Source	1%
5	www.nature.com Internet Source	<1%
6	Wee-Jun Ong, Lling-Lling Tan, Yun Hau Ng, Siek-Ting Yong, Siang-Piao Chai. " Graphitic	<1%

	Carbon Nitride (g-C N)-Based Photocatalysts for Artificial Photosynthesis and Environmental Remediation: Are We a Step Closer To Achieving Sustainability? ", Chemical Reviews, 2016 Publication	
7	link.springer.com Internet Source	<1 %
8	Yolanda Rati, Yasni Novi Hendri, Rachmat Waluyo, Febriman Zendrato et al. "Visible light assisted degradation of Rhodamin B by reusable S-doped ZnO thin film photocatalyst", Optical Materials, 2023 Publication	<1 %
9	www.hindawi.com Internet Source	<1 %
10	f1000research.com Internet Source	<1 %
11	gyan.iitg.ac.in Internet Source	<1 %
12	d-nb.info Internet Source	<1 %
13	www2.mdpi.com Internet Source	<1 %
14	Qingzhao Liao, Yanling Wu, Xianrui Chen, Yifeng Huang, Mengxue Xu, Chunye Nong, Xiaojing Gao, Zhimin Huang, ning xiao. "Microbially Induced Sand Cementation Using	<1 %

Lysinibacillus fusiformis NM01", Springer Science and Business Media LLC, 2025
Publication

15	etheses.whiterose.ac.uk Internet Source	<1 %
16	Akash D. Salmote, Abhijeet R. Pawar, Kahkashan R. Shaikh, Prabhakar B. Undre. "Enhanced photocatalytic degradation of crystal violet with hexagonal nanosheets of Cu-doped Co3O4 underUVandvisible irradiation", Journal of Materials Science: Materials in Electronics, 2025 Publication	<1 %
17	Manoj Kumar, Atikur Rahman, Tahir Ahmad Dar, Ayush Chandra Pundir. "Design and development of La_2O_3-doped ZnO p–n heterostructures: structural, optical, and photocatalytic properties for dye degradation applications", Optical and Quantum Electronics, 2025 Publication	<1 %
18	Submitted to Nottingham Trent University Student Paper	<1 %
19	www.rsc.org Internet Source	<1 %
20	David Jereil S, Shankar S M, Sudhakar K, Ganeshkumar Arumugam et al. "Effect of Cu-ZnO nanoparticles on the photocatalytic	<1 %

degradation of reactive red 120", Surfaces and Interfaces, 2025
Publication

21	Submitted to Kuwait University Student Paper	<1%
22	iwaponline.com Internet Source	<1%
23	Submitted to Higher Education Commission Pakistan Student Paper	<1%
24	Submitted to Tikrit University Student Paper	<1%
25	coloringfolder.com Internet Source	<1%
26	nrc-publications.canada.ca Internet Source	<1%
27	cheap-buy.t35.com Internet Source	<1%
28	www.hexarelin.us Internet Source	<1%
29	www.researchgate.net Internet Source	<1%
30	Huifang Wu, Jiahui Jiang, Xiaoting Gu, Changlun Tong. "Nitrogen and sulfur co-doped carbon quantum dots for highly selective and sensitive fluorescent detection	<1%

of Fe(III) ions and L-cysteine", Microchimica Acta, 2017
Publication

31	journals.uob.edu.bh Internet Source	<1%
32	Alexandre I. Danilov. "Ultrastructural and antigenic properties of neural stem cells and their progeny in adult rat subventricular zone", Glia, 01/15/2009 Publication	<1%
33	Li Li, Lu Pan, Dawen Zhang, Jiewei Rong. "Ultrasonic-assisted synthesis of LaFeO3/CeO2 heterojunction for enhancing the photocatalytic degradation of organic pollutants", Materials Science in Semiconductor Processing, 2022 Publication	<1%
34	Roberto A. Colina-Ruiz, Juan A. Hoy-Benítez, Juan S. Lezama-Pacheco, José Mustre de León, Francisco J. Espinosa-Faller. "Local atomic structure and Ni nanophase segregation in Zn1-xNixS thin films", Journal of Alloys and Compounds, 2020 Publication	<1%
35	datapdf.com Internet Source	<1%
36	doczz.net Internet Source	<1%

pubmed.ncbi.nlm.nih.gov

37	Internet Source	<1%
38	www.ncbi.nlm.nih.gov Internet Source	<1%
39	www.thno.org Internet Source	<1%
40	Ahmad Umar, Siddheshwar D. Raut, Ahmed A. Ibrahim, Hassan Algadi et al. "Perforated Co3O4 nanosheets as high-performing supercapacitor material", Electrochimica Acta, 2021 Publication	<1%
41	Thu Ha Thi Vu, Thao Thi Nguyen, Tien Hoang Nguyen, Minh Dang Nguyen, Quang Minh Nguyen. "A new method for synthesizing high performance few-layer graphene supported Pt electrocatalysts in methanol and ethanol oxidation", Electrochimica Acta, 2021 Publication	<1%
42	c.coek.info Internet Source	<1%
43	core.ac.uk Internet Source	<1%
44	digitalcommons.lib.uconn.edu Internet Source	<1%
45	digitallibrary.tulane.edu Internet Source	<1%

46	downloads.hindawi.com Internet Source	<1%
47	Ziye Shen, Hongyu Zhou, Peng Zhou, Heng Zhang, Zhaokun Xiong, Yahan Yu, Gang Yao, Bo Lai. "Degradation of atrazine in water by Bi2MoO6 and visible light activated Fe3+/peroxymonosulfate coupling system", Journal of Hazardous Materials, 2022 Publication	<1%

Exclude quotes	On	Exclude matches	< 5 words
Exclude bibliography	On		